nature genetics

SUPPLEMENTARY INFORMATION

https://doi.org/10.1038/s41588-018-0221-x

In the format provided by the authors and unedited.

Dynamic 3D chromatin architecture contributes to enhancer specificity and limb morphogenesis

Bjørt K. Kragesteen[1,2,3,4,14], Malte Spielmann[1,2,14], Christina Paliou[1,2,3], Verena Heinrich[5], Robert Schöpflin[1,2,5], Andrea Esposito[6,7], Carlo Annunziatella[6], Simona Bianco[6], Andrea M. Chiariello[6], Ivana Jerković[1,4], Izabela Harabula[1], Philine Guckelberger[1], Michael Pechstein[1], Lars Wittler[8], Wing-Lee Chan[2], Martin Franke[1,2,3], Darío G. Lupiáñez[1,2,3,9], Katerina Kraft[1,2,3], Bernd Timmermann[10], Martin Vingron[5], Axel Visel[11,12,13], Mario Nicodemi[6,7*], Stefan Mundlos[1,2,3*] and Guillaume Andrey[1,2,3*]

[1]RG Development & Disease, Max Planck Institute for Molecular Genetics, Berlin, Germany. [2]Institute for Medical and Human Genetics, Charité-Universitätsmedizin Berlin, Berlin, Germany. [3]Berlin-Brandenburg Center for Regenerative Therapies, Charité-Universitätsmedizin Berlin, Berlin, Germany. [4]Berlin-Brandenburg School for Regenerative Therapies, Charité-Universitätsmedizin Berlin, Berlin, Germany. [5]Department of Computational Molecular Biology, Max Planck Institute for Molecular Genetics, Berlin, Germany. [6]Dipartimento di Fisica, Università di Napoli Federico II, and Istituto Nazionale di Fisica Nucleare, Napoli, Complesso Universitario di Monte Sant'Angelo, Naples, Italy. [7]Berlin Institute of Health, MDC-Berlin, Berlin, Germany. [8]Department of Developmental Genetics, Max Planck Institute for Molecular Genetics, Berlin, Germany. [9]Epigenetics and Sex Development Group, Berlin Institute for Medical Systems Biology, Max-Delbrück Center for Molecular Medicine, Berlin-Buch, Germany. [10]Max Planck Institute for Molecular Genetics, Sequencing Core Facility, Berlin, Germany. [11]Lawrence Berkeley National Laboratory, Berkeley, CA, USA. [12]U.S. Department of Energy Joint Genome Institute, Walnut Creek, CA, USA. [13]School of Natural Sciences, University of California, Merced, CA, USA. [14]These authors contributed equally: Bjørt K. Kragesteen, Malte Spielmann. *e-mail: nicodem@na.infn.it; mundlos@molgen.mpg.de; andrey@molgen.mpg.de

A

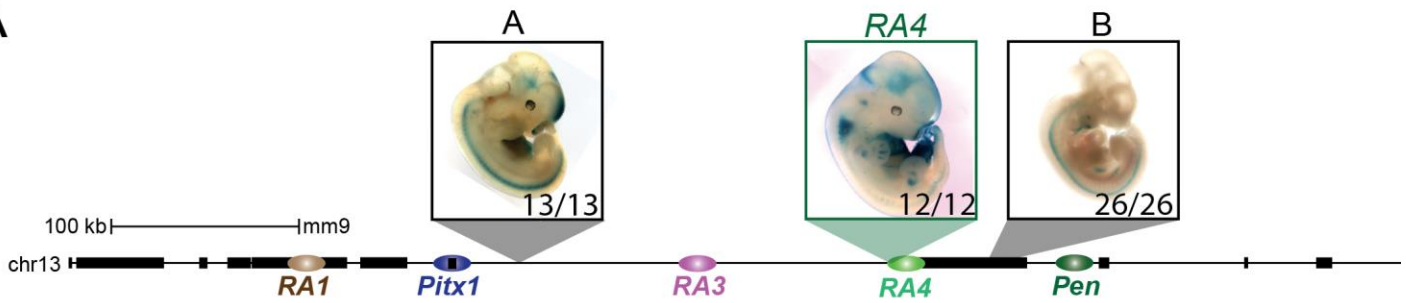

Putative enhancer region	Chr coordinates (mm9)	Staining pan limb	Staining first branchial arch	Radke's pouch	Staining gut	Other
A	chr13:55,999,701-56,001,600	no	no	no	no	yes
B	chr13:56,212,475-56,215,363	no	yes	no	yes	yes
Pit	chr13:56,062,458-56,064,945	no	no	yes	no	yes
RA4	chr13:56,167,110-56,172,034	yes	no	no	no	yes
Pen	chr13:56,260,379-56,262,548	yes	no	no	no	yes

B

LacZ-Sensor	Chr coordinates (mm9) of insertion	Staining pan limb	Staining first branchial arch	Radke's pouch	Staining gut	Other
1	chr13:55,935,387	no	yes	yes	yes	yes
2	chr13:56,257,249	yes	no	no	no	no

Supplementary Figure 1

Probing the regulatory sequences and activities of the *Pitx1* locus.

a, Table listing putative enhancer regions tested by *lacZ* reporter assay. Above is the *lacZ* reporter activity in E11.5 embryos. Numbers represent the number of embryos displaying the staining shown in the table. **b**, Table listing the genomic location of *lacZ* sensors 1 and 2 at the *Pitx1* locus (mm9) and *lacZ* reporter staining in E11.5 embryos.

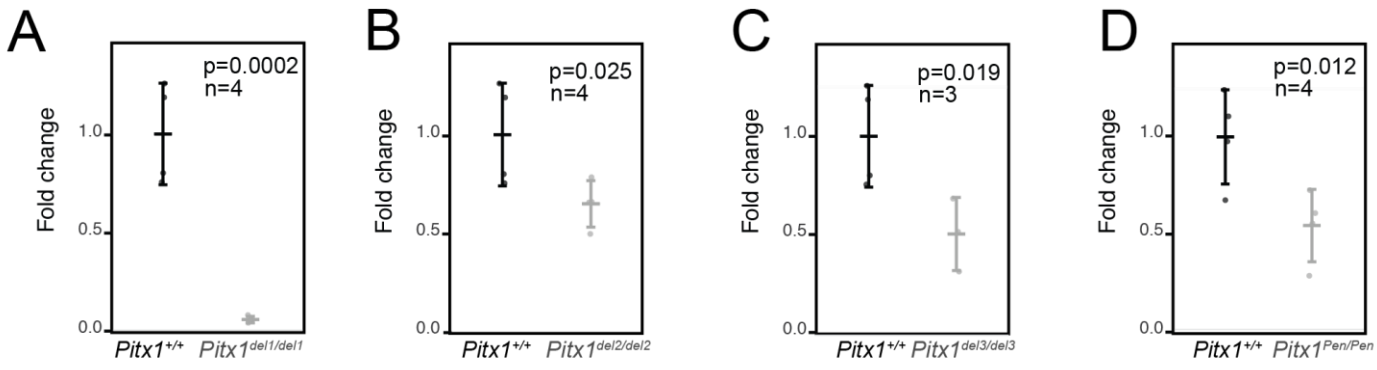

Supplementary Figure 2

Quantification of *Pitx1* hindlimb transcription in several deletion mice.

In all analyses, we used a one-sided *t* test to evaluate the significance of the decrease in *Pitx1* expression and *n* represents the number of wild-type and mutant hindlimb pairs assayed. The s.d. is displayed as error bars and the measure of the center corresponds to the average. **a**, qRT–PCR mRNA quantification of E11.5 *Pitx1*$^{del1/del1}$ hindlimbs (P = 0.0002, n = 4). **b**, qRT–PCR mRNA quantification of E11.5 *Pitx1*$^{del2/del2}$ hindlimbs (P = 0.025, n = 4). **c**, qRT–PCR mRNA quantification of E11.5 *Pitx1*$^{del3/del3}$ hindlimbs (P = 0.019, n = 3). **d**, qRT–PCR mRNA quantification of E11.5 *Pitx1*$^{Pen/Pen}$ hindlimbs (P = 0.012, n = 4).

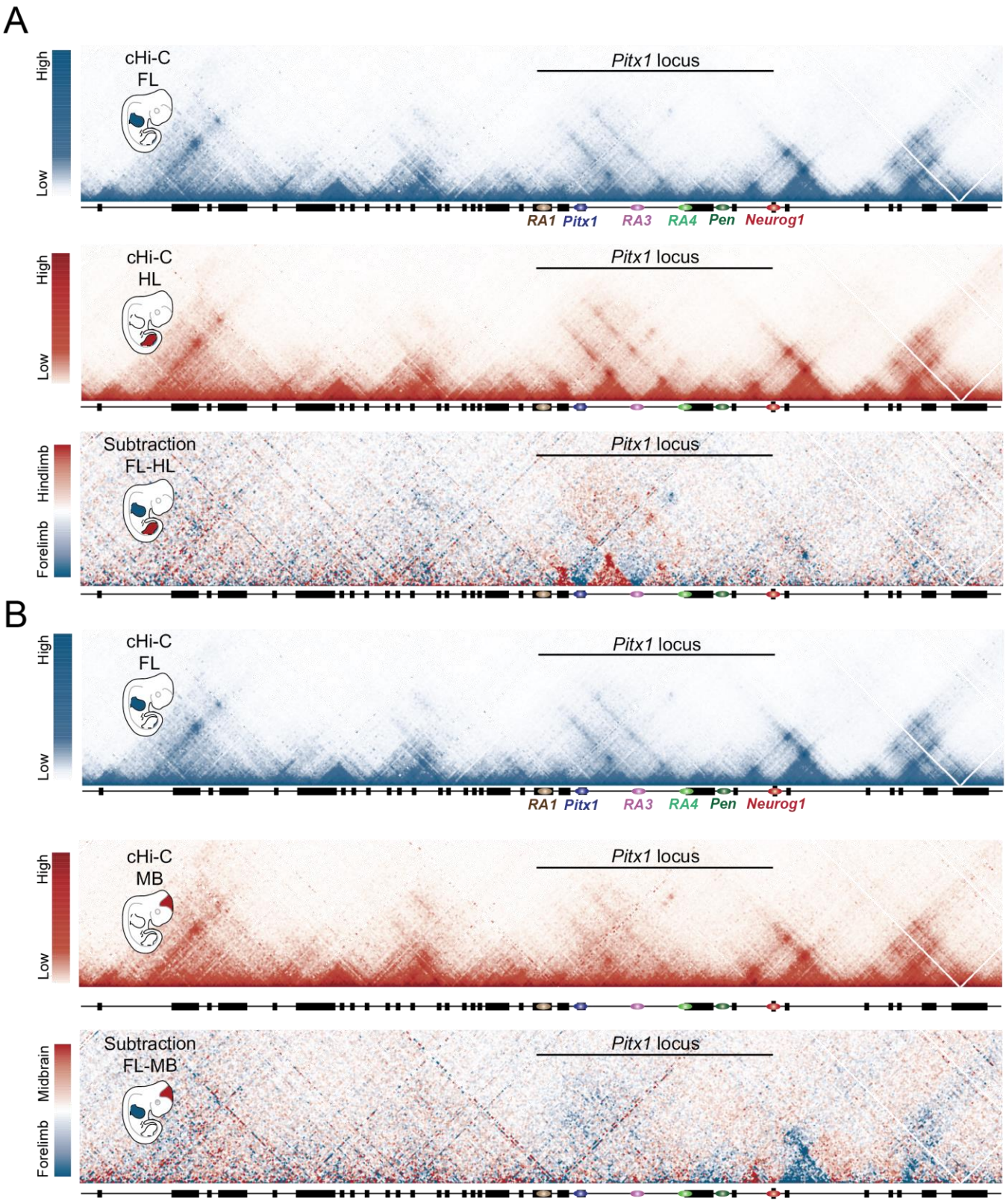

Supplementary Figure 3

cHi-C of the extended *Pitx1* locus in wild-type forelimb, hindlimb and midbrain tissues.

a, cHi-C interaction map in E11.5 forelimb (blue) and hindlimb (red) tissues over a 3-Mb captured region. Bottom, subtraction of hindlimb and forelimb cHi-C whereby blue indicates a higher chromatin interaction frequency in forelimb and red a higher interaction frequency in hindlimb as compared to each other. Note that only the *Pitx1* locus displays clear changes in chromatin interactions within the entire captured region. **b**, cHi-C interaction map in E11.5 forelimb (blue) and E10.5 midbrain (red) tissues over a 3-Mb captured region. Bottom, subtraction of midbrain and forelimb cHi-C whereby blue indicates a higher chromatin interaction frequency in forelimb and red a higher interaction frequency in midbrain as compared to each other. Note the absence of chromatin interaction changes at the *Pitx1* locus, in contrast to the neighboring telomeric domain (see blue domain in subtraction map), which include *Cxcl14*, a gene transcriptionally repressed in midbrain and active in forelimb.

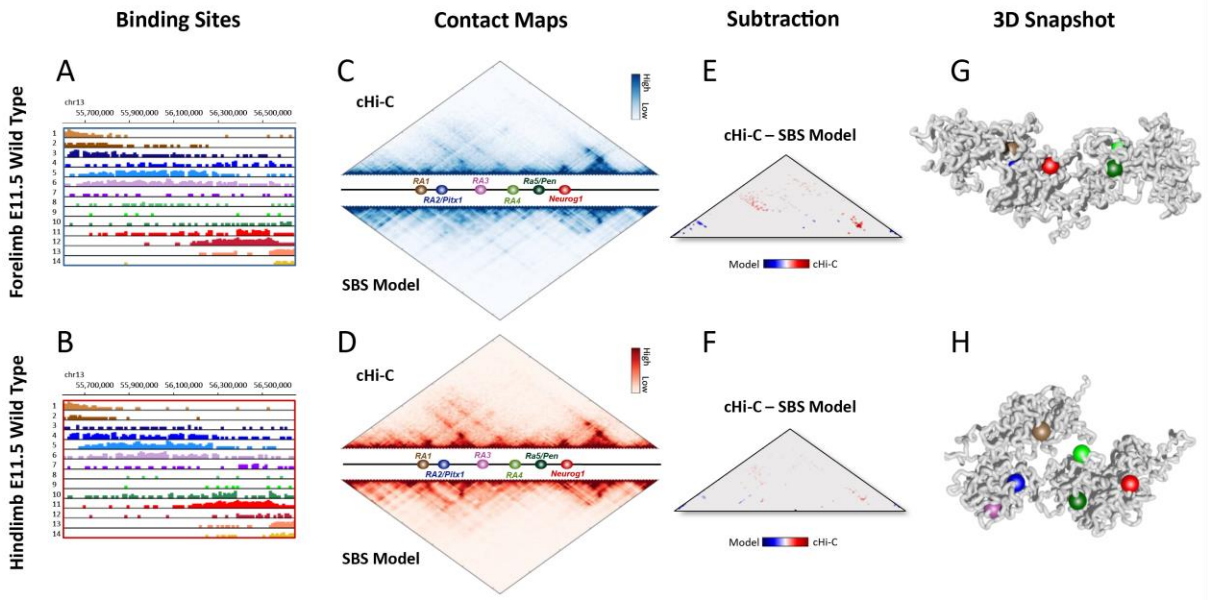

Supplementary Figure 4

Modeling of the *Pitx1* locus 3D architecture in wild-type forelimb and hindlimb.

a,**b**, Histograms displaying the position and abundance of 14 different types of binding sites (Methods) along the genome, in forelimbs (top) and hindlimbs (bottom) as derived from the E11.5 cHi-C data. Each binding site is displayed with a different color. **c**,**d**, Contact maps derived from cHi-C (above) and SBS model (below) display high similarity. The Pearson correlation, *r*, and the genomic-distance-corrected Pearson correlation, *r′*, between the cHi-C and SBS matrices (105 bins × 105 bins = 11,025) are $r = 0.98$ and $r' = 0.84$ in forelimb and $r = 0.98$ and $r' = 0.82$ in hindlimb. **e**,**f**, Subtraction matrices between cHi-C and SBS model in wild-type forelimbs (top) and hindlimbs (bottom). Differences above random background are shown in red and blue. **g**,**h**, A representative 3D structure of the locus in forelimb (top) and hindlimb (bottom), selected from the ensemble of ‘single-cell’ model-derived conformations (Methods). In Fig. 4d,e, the corresponding coarse-grained versions are shown to highlight the position of genes and regulators.

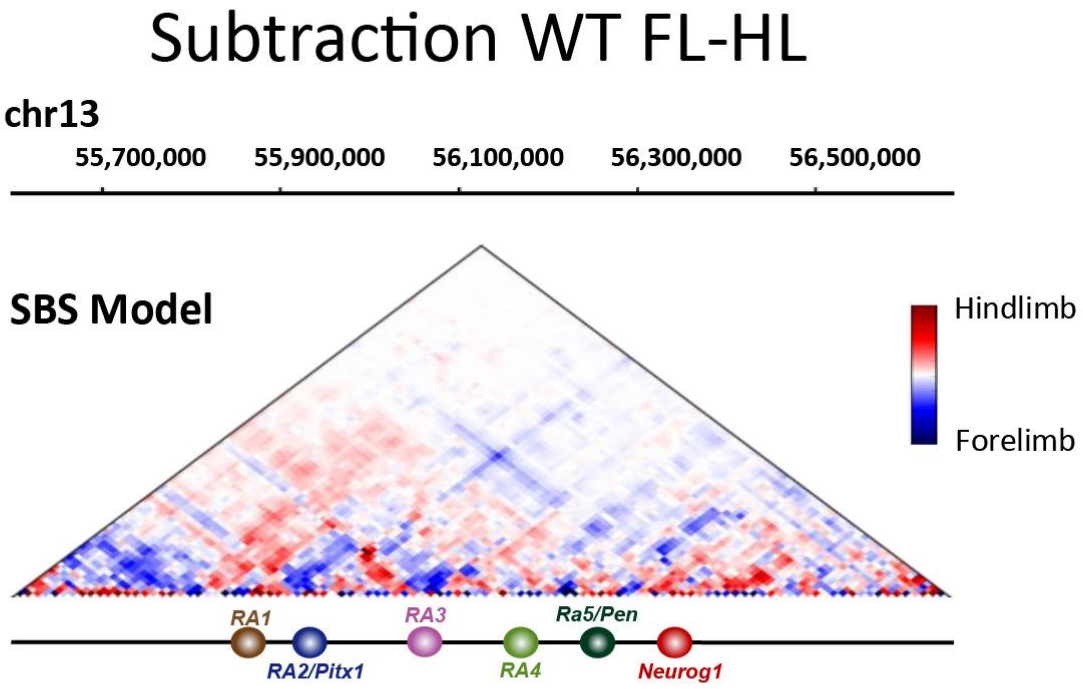

Supplementary Figure 5

Subtraction matrix between the SBS models of wild-type forelimb and hindlimb.

The corresponding cHi-C data are shown in Fig. 4c.

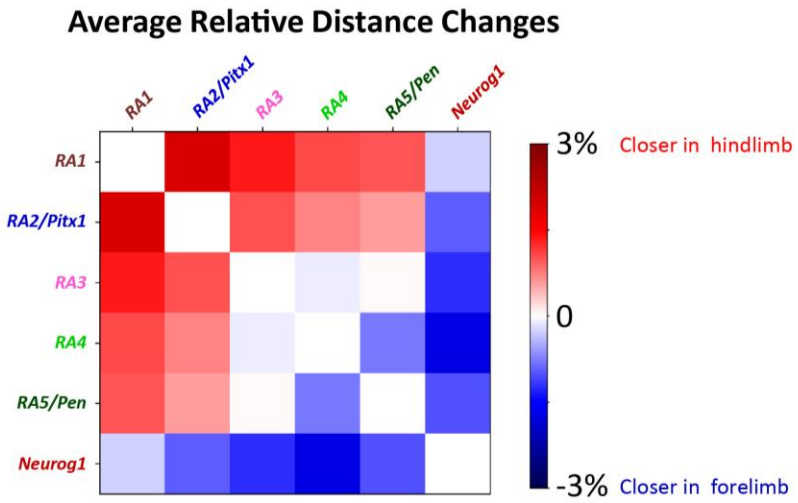

Supplementary Figure 6

Relative changes in physical distances between wild-type forelimb and hindlimb 3D structure.

Heat map showing relative changes in physical distances between forelimb and hindlimb 3D structure as measured by the polymer model.

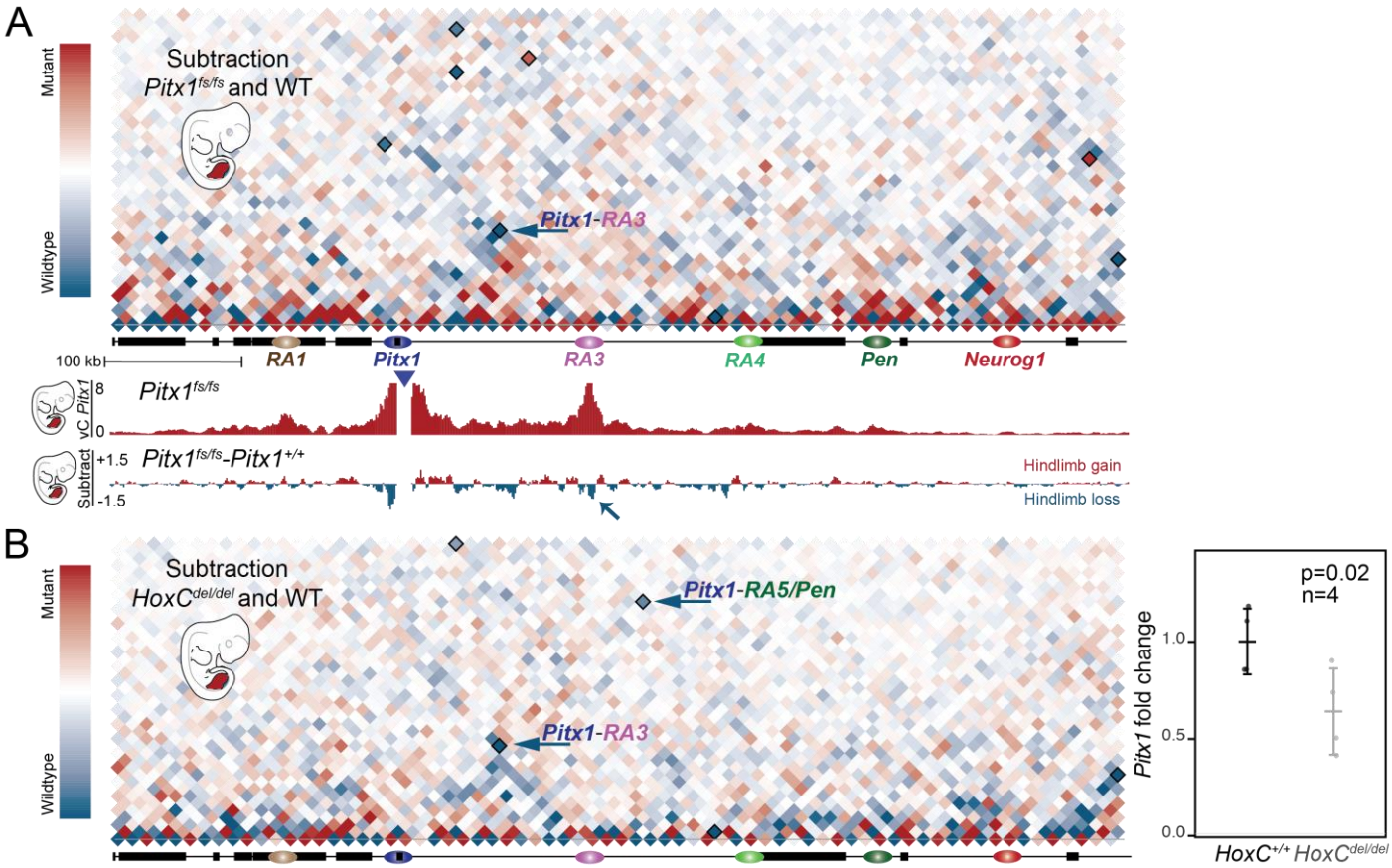

Supplementary Figure 7

Effect of *Pitx1* and *HoxC* loss of function on the 3D structure of the *Pitx1* locus in hindlimbs.

a, cHi-C subtraction between wild-type and *Pitx1*$^{fs/fs}$ mutant hindlimb tissue at E11.5. Chromatin interactions more prevalent in mutant or wild-type hindlimb tissues are shown in red and blue, respectively. Significant changes in interactions are highlighted in black boxes (FDR = 0.05). Interactions significantly reduced between regulatory anchors are indicated with a blue arrow (*Pitx1–RA3* interaction). Derived viewpoint from cHi-C map, vC, using the *Pitx1* viewpoint is shown in red. Below is the subtraction track between wild-type and mutant hindlimb tissues using the respective viewpoint. **b**, cHi-C subtraction between wild-type and *HoxC*$^{del/del}$ mutant hindlimb tissues at E11.5. Chromatin interactions more prevalent in mutant or wild-type hindlimb tissues are shown in red and blue, respectively. Significant changes are highlighted in black boxes (FDR = 0.05). Interactions significantly reduced between regulatory anchors are indicated with blue arrows (*Pitx1–RA3* and *Pitx1–Pen*). qRT–PCR quantification of *Pitx1* in *HoxC*$^{del/del}$ mutant hindlimb tissues at E11.5 showed an average 36% reduction. (We used a one-sided *t* test to evaluate the significance of decrease in *Pitx1* expression and found $P = 0.02$; $n = 4$ wild-type and mutant hindlimb pairs; s.d. is displayed as error bars; the measure of the center is the average of the data points.)

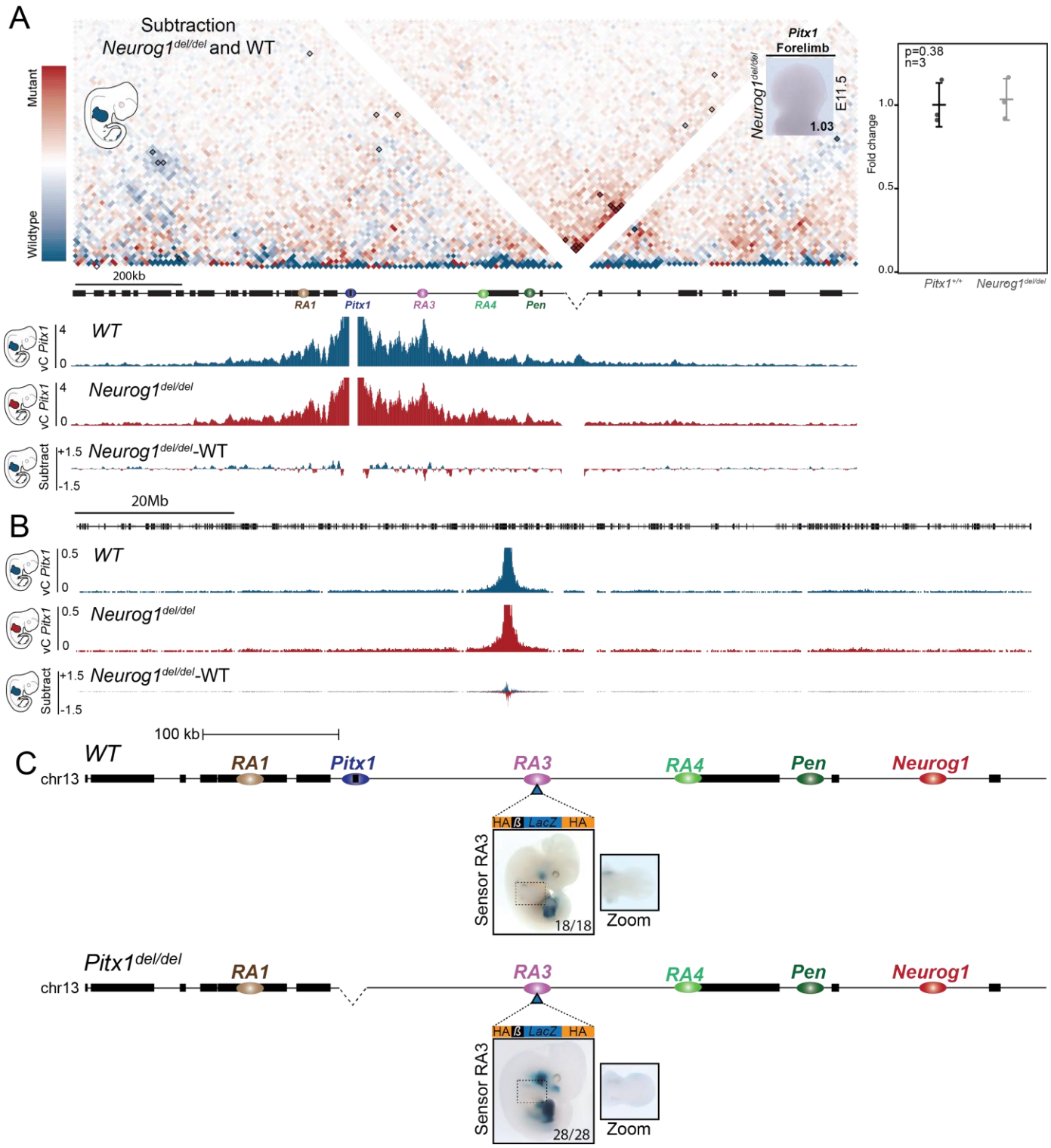

Supplementary Figure 8

Deletions of the *Pitx1* or *Neurog1* H3K27me3 domains are not sufficient to perturb the hindlimb-restricted regulatory activity of the locus.

a, cHi-C subtraction between wild-type and *Neurog1*$^{del/del}$ mutant forelimb tissue at E11.5. Chromatin interactions more prevalent in mutant or wild-type forelimb tissues are shown in red and blue, respectively. Significant changes are highlighted in black boxes (FDR =

0.05). Right, *Neurog1*$^{del/del}$ embryos do not show changes in *Pitx1* expression in E11.5 forelimbs as seen in WISH (photo) and quantified by qRT–PCR. (We used a one-sided *t* test to evaluate the significance of increased *Pitx1* expression and found $P = 0.38$; $n = 3$ wild-type and mutant limb pairs; the center is the average and the s.d. is displayed by the error bars.) Below, derived vC from the *Pitx1* viewpoint in wild-type and *Neurog1*$^{del/del}$ forelimbs are shown in blue and red, respectively. Below is the subtraction track between wild-type and mutant forelimb tissue using the respective viewpoint. **b**, Whole chromosome 13 view of vC from the *Pitx1* viewpoint. Note that these profiles display the genomic region enriched in cHi-C as well as the non-enriched part of the chromosome. **c**, Staining of embryos with a *lacZ* sensor integrated in the *RA3* region. Wild-type (top) and *Pitx1*$^{del/del}$ (bottom) staining display no obvious difference between fore- and hindlimb. Eighteen of 18 embryos displayed the same staining in the wild-type background, and 28 of 28 displayed the same staining in the *Pitx1*$^{del/del}$ background.

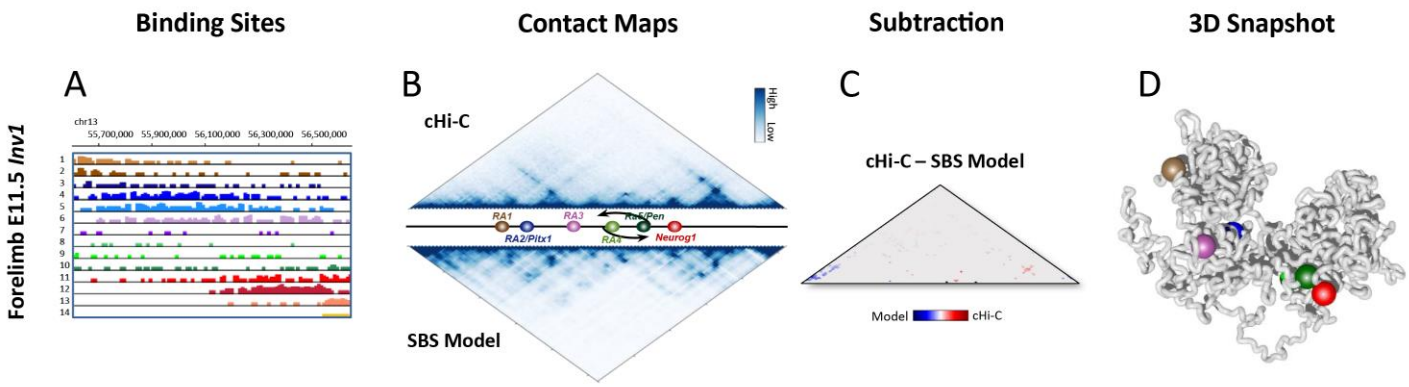

Supplementary Figure 9

Modeling of the *Pitx1* locus 3D architecture in *Pitx1*$^{inv1/inv1}$ forelimbs.

a, Histograms displaying the position and abundance of 14 different types of binding sites (Methods) along the genome, in *Pitx1*$^{inv1/inv1}$ forelimbs at E11.5. As in Supplementary Fig. 4a,b, each binding site is displayed with a different color. **b**, Contact maps derived from cHi-C (above) and SBS model (below) display high similarity. The Pearson correlation, *r*, and the genomic-distance-corrected Pearson correlation, *r′*, between the cHi-C and SBS matrices (105 bins * 105 bins = 11,025) are $r = 0.97$ and $r' = 0.74$. **c**, Subtraction matrix between cHi-C and SBS model in *Pitx1*$^{inv1/inv1}$ forelimbs. Differences above random background are shown in red and blue. **d**, A representative 3D structure of the locus in *Pitx1*$^{inv1/inv1}$ forelimbs, selected from the ensemble of 'single-cell' model-derived conformations (Methods). In Fig. 6e, the corresponding coarse-grained version is shown to highlight the position of genes and regulators.

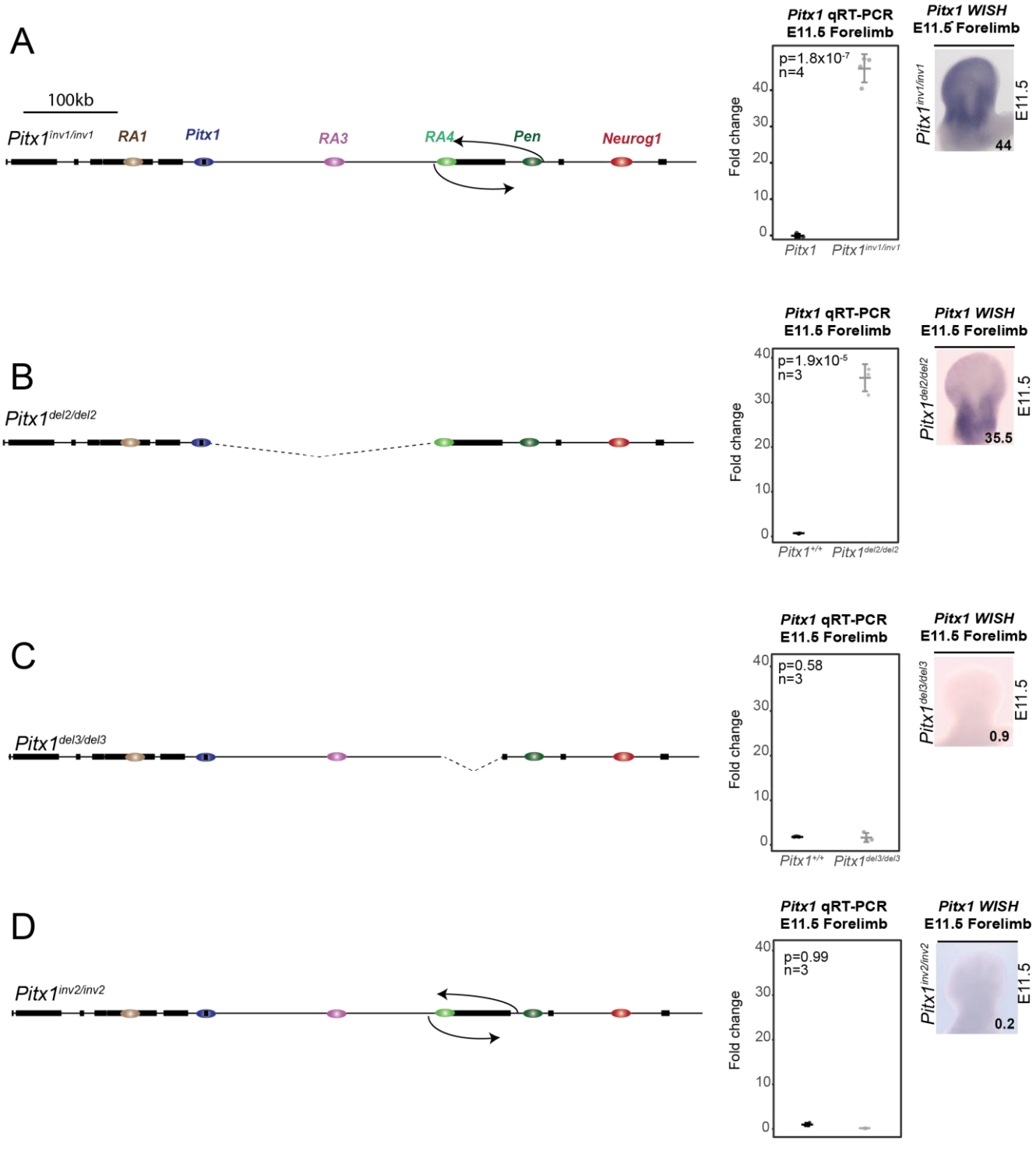

Supplementary Figure 10

Quantification of *Pitx1* forelimb transcription in several deletion and inversion mice.

WISH and qRT–PCR mRNA quantification of deletions and inversion at the *Pitx1* locus. In all analyses, we used a one-sided *t* test to evaluate the significance of increased *Pitx1* expression and *n* represents the number of wild-type and mutant forelimb pairs assayed. The s.d. is displayed as error bars and the measure of the center corresponds to the average. **a**, WISH and qRT–PCR mRNA quantification of E11.5 $Pitx1^{inv1/inv1}$ forelimbs ($P = 1.8 \times 10^{-7}$, $n = 4$). **b**, WISH and qRT–PCR mRNA quantification of E11.5 $Pitx1^{del2/del2}$ forelimbs ($P = 1.9 \times 10^{-5}$, $n = 3$). **c**, WISH and qRT–PCR mRNA quantification of E11.5 $Pitx1^{del3/del3}$ forelimbs ($P = 0.58$, $n = 3$). **d**, WISH and qRT–PCR mRNA quantification of E11.5 $Pitx1^{inv2/inv2}$ forelimbs ($P = 0.99$, $n = 3$).

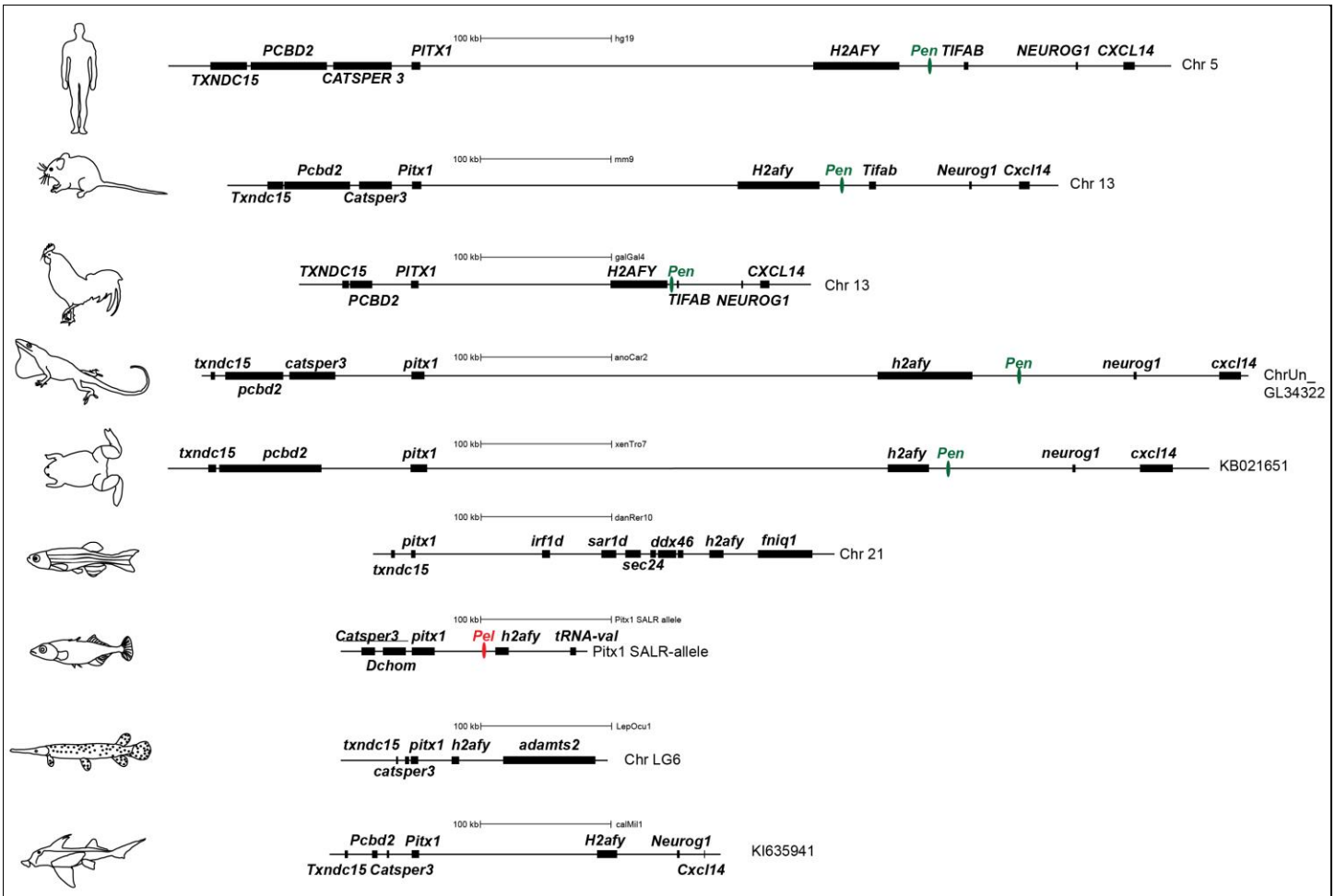

Supplementary Figure 11

Schematic representation of the *Pitx1* locus in several species.

Schematic representation of the *Pitx1* extended locus in several species, demonstrating the conserved synteny of the region. The speciesrom top to bottom are human (*Homo sapiens*), mouse (*Mus musculus*), chicken (*Gallus gallus*), lizard (*Anolis carolinensis*), frog (*Xenopus (Silurana) tropicalis),* zebrafish (*Danio rerio*), stickleback (*Gasterosteus aculeatus*), spotted gar (*Lepisosteus oculatus*), and elephant shark (*Callorhinchus milii*). *Pen* (green) is found in tetrapods but not in fish. The previous characterized pelvic enhancer *Pel* (red) is displayed in red in stickleback.

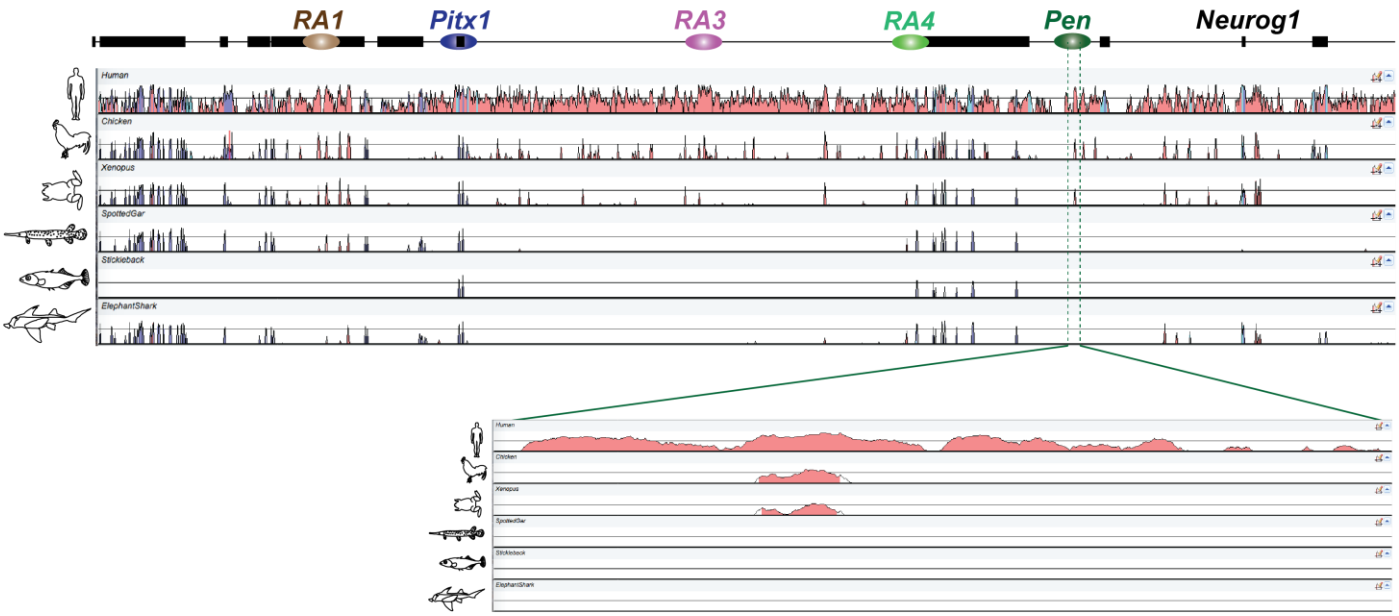

Supplementary Figure 12

Conservation of sequences between vertebrates along the *Pitx1* regulatory landscape.

Conservation of sequences between vertebrates along the *Pitx1* regulatory landscape. A zoomed-in view of the *Pen* region shows that the element is conserved with human (*Homo sapiens*), chicken (*Gallus gallus*), and frog (*Xenopus (Silurana) tropicalis*), but not with bony or cartilaginous fishes (here stickleback (*Gasterosteus aculeatus*), spotted gar (*Lepisosteus oculatus*), and elephant shark (*Callorhinchus milii*).